Journal of Power Sources 234 (2013) 107–110

Contents lists available at SciVerse ScienceDirect

Journal of Power Sources

journal homepage: www.elsevier.com/locate/jpowsour

Short communication

Supercapacitive evaluation of soft chemically deposited α-Sm_2S_3 thin films

V.S. Kumbhar, A.D. Jagadale, C.D. Lokhande*

Thin Film Physics Laboratory, Department of Physics, Shivaji University, Kolhapur 416 004, Maharashtra, India

HIGHLIGHTS

► The preparation of samarium trisulphide material in thin film form at room temperature.
► A porous honeycomb like morphology of the samarium trisulphide thin film.
► An application of the film as an electrode in supercapacitor cell.

ARTICLE INFO

Article history:
Received 7 December 2012
Received in revised form
13 January 2013
Accepted 15 January 2013
Available online 22 January 2013

Keywords:
α-Sm_2S_3
Thin films
Nanoporous
Supercapacitor
Scanning electron microscopy
Cyclic voltammetry

ABSTRACT

The nanoporous honeycomb like binary α-Sm_2S_3 material is used as supercapacitor electrode. The soft chemical, successive ionic layer adsorption and reaction (SILAR) method is employed for the α-Sm_2S_3 thin film growth. The synthesised films are characterised by X-ray diffraction (XRD) and scanning electron microscopy (SEM) for structural and morphological studies. Electrochemical behaviour is studied using cyclic voltammetry (CV), galvanostatic charge–discharge and electrochemical impedance spectroscopy (EIS). The observed specific and interfacial capacitance (C_s and C_i) values in 1 M $LiClO_4$ –propylene carbonate (PC) electrolyte are 294 F g^{-1} and 0.0238 F cm^{-2}, respectively at the scan rate of 5 mV s^{-1}. An electrode stability of 89% retained after 1000 cycles. A galvanostatic charge–discharge and EIS study show ideal capacitive behaviour of α-Sm_2S_3 electrode.

1. Introduction

The supercapacitors, also called as electrochemical capacitors have been attracting great attention of researchers all over the world for high power density and long cycle life. These fill the gap between electrolytic capacitors (high power density devices) and battery (high energy density devices) [1]. Generally, supercapacitors have been classified into three main types on the basis of charge storage mechanism at the electrode–electrolyte interface. They are electrochemical double layer capacitors (EDLC), where no chemical reaction occurs at an electrode; thereby the charge is stored non-faradically at an interface, leading to excellent stability of an electrode. These include carbon based materials and nowadays efforts have been going on to achieve the higher surface area by employing different preparative methods [2,3]. The second type of supercapacitors is pseudocapacitors which uses reduction and oxidation reactions to store charge at an electrode interface. These involve metal oxides like Co_3O_4 [4] V_2O_5 [5] etc. In addition, conducting polymers also show pseudocapacitive behaviour, but their performance is poor with respect to stability. The last type involves the combination of EDLC and pseudocapacitor called as hybrid supercapacitors in which people try to make use of strength and the high surface area of carbon materials to deposit inorganic materials over it and thereby overall performance is improved [6]. The recent research is focused onto finding a new material which can show better cycling stability with high values of capacitance.

Metal sulphides have been emerging as one of the new class of material in various applications such as solar cells [7], thermoelectrics [8] etc. There are few reports available on the supercapacitive study of metal sulphides prepared via hydrothermal [9] and solvothermal methods [10] and no reports are available on the supercapacitive behaviour of rare earth sulphides. One of the rare earth sulphides, the sulphide of samarium exits in different phases such as SmS, Sm_2S_3, Sm_3S_4 etc. depending upon preparative

* Corresponding author. Tel.: +91 231 2609225.
E-mail address: l_chandrakant@yahoo.com (C.D. Lokhande).

0378-7753/$ – see front matter © 2013 Elsevier B.V. All rights reserved.
http://dx.doi.org/10.1016/j.jpowsour.2013.01.078

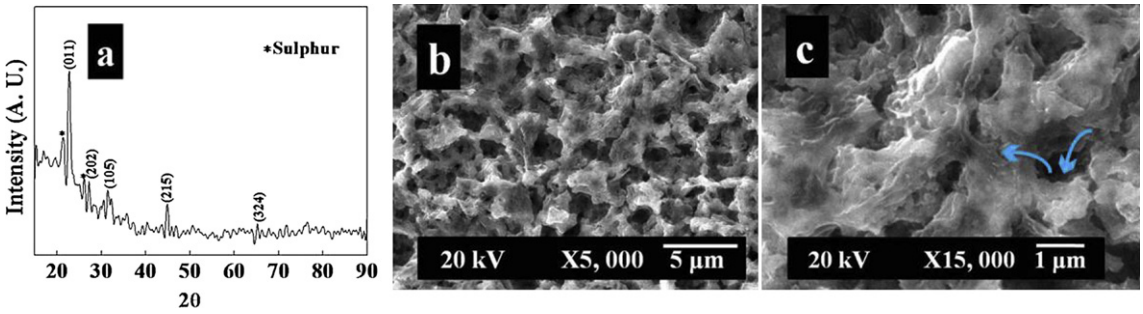

Fig. 1. (a) The XRD pattern of α-Sm_2S_3 material, (b) the SEM image of α-Sm_2S_3 thin film at magnifications of ×5000 and (c) ×15,000.

conditions. Out of which SmS exhibits semiconductor to metal transition by the application of pressure and vice-versa [11], whereas Sm_3S_4 shows thermoelectric behaviour [12]. The literature survey reveals that there are no reports on the applicative properties of Sm_2S_3 except as a photoelectrochemical solar cell [13].

In this article, we report for the first time, on the supercapacitive behaviour of α-Sm_2S_3 thin film. The films are characterised using X-ray diffraction (XRD) and scanning electron microscopy (SEM) techniques. The cyclic voltammetry (CV), galvanostatic charge–discharge and electrochemical impedance spectroscopy (EIS) are utilised to study supercapacitive properties of the film.

2. Experimental

The commercially available AR grade samarium oxide (Sm_2O_3), tartaric acid ($C_4H_6O_6$) and sodium thiosulphate ($Na_2S_2O_3$) were employed for the deposition. Sm_2O_3 was complexed using 0.25 M $C_4H_6O_6$ to get 10 ml of 0.1 M $SmCl_3$ (pH = 2) as a cationic source. A 0.15 M of 10 ml $Na_2S_2O_3$ (pH = 2) was used as an anionic source for sulphide ions. The four steps were used in depositing the α-Sm_2S_3 film. First, the substrate was dipped in cationic bath for 40 s, so as to adsorb the Sm^{3+} ions onto the substrate, subsequently; it was rinsed in double distilled water for 20 s to remove excess loosely adsorbed ions. Then, it was dipped in anionic precursor for 40 s to react S^{2-} ion with previously adsorbed Sm^{3+} ions. Finally, it was rinsed in double distilled water for 20 s to remove unreacted S^{2-} ions, completing single cycle. These cycles were repeated to get optimized film thickness of 0.18 mg cm^{-2}.

The XRD measurement was carried on a Bruker D-8 diffractometer using Cu Kα (λ = 1.54 Å) radiation. The surface morphology of sample was studied using scanning electron microscope (JEOL 6360, Japan). The CV and galvanostatic charge–discharge measurements were carried out using (WBCS 3000) automatic battery cycler system in non-aqueous $LiClO_4$–propylene carbonate (PC) electrolyte. An impedance analyzer (model, CHI6112D) was employed to obtain different supercapacitive parameters of α-Sm_2S_3 thin film electrode in same electrolyte using three electrode system.

3. Results and discussion

3.1. Structural studies

The XRD pattern of α-Sm_2S_3 material is reflected in Fig. 1(a). The existence of Sm-S system in different forms such as SmS, β-Sm_2S_3, Sm_3S_4 etc. depends upon the synthesis conditions such as starting materials, temperature of synthesis and synthesis method employed [14]. The formation of sulphur as an impurity phase is detected from the reflections at 21.4 and 26.1°, whereas the peaks at 22.7, 27.2, 31.5, 44.8 and 65.2° correspond to orientation of the α-Sm_2S_3 along (011), (202), (105), (215) and (324) planes, respectively. These peak positions are in good agreement with standard α-Sm_2S_3 material peaks (JCPDS card No. 44-1259). The Scherer formula is used to determine crystallite size as follows,

$$D = \frac{0.9\lambda}{\beta \cos\theta} \quad (1)$$

where, the symbols have their usual meanings. The particle size obtained is 470 nm for the plane (011).

3.2. SEM studies

The surface morphology of a thin film plays a vital role in supercapacitive behaviour of material, since better surface morphology provides high surface area. Consequently, more number of redox sites will be made available during charge–discharge of a supercapacitor cell. The scanning electron microscope images of α-Sm_2S_3 film surface taken at 5 K× and 15 K× magnifications are indicated in Fig. 1(b) and (c) respectively. Patil et al. [15] synthesised similar kind of porous NiO honeycomb by chemical bath deposition. The non-uniform sized pores ranging from 0 to 1 μm are observed

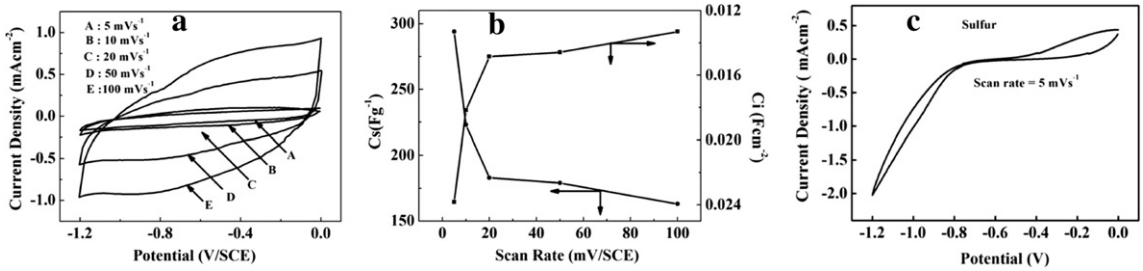

Fig. 2. (a) The cyclic voltammograms of α-Sm_2S_3 film electrode at different scan rates in working potential window of 0 V to −1.2 V SCE^{-1}, (b) variation C_s and C_i capacitances of α-Sm_2S_3 thin film electrode at different scan rates and (c) the cyclic voltammogram of sulphur at the scan rate of 5 mV s^{-1} in working potential window of 0 to −1.2 V SCE^{-1}.

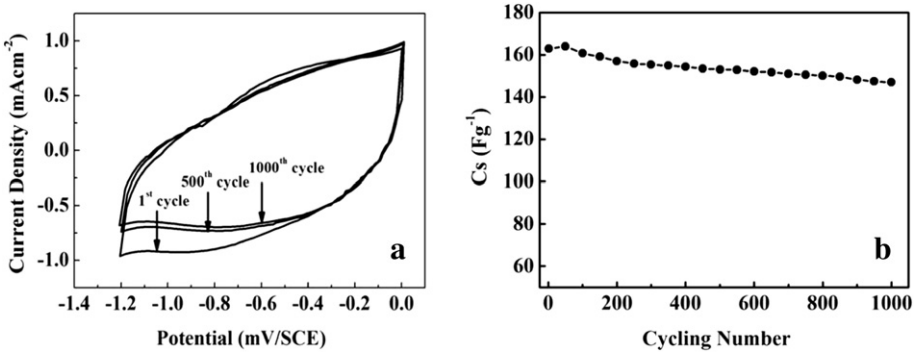

Fig. 3. (a) Electrochemical stability α-Sm_2S_3 film electrode at scan rate of 100 mV s^{-1} at 1st, 500th and 1000th cycles and (b) variation of C_s with respect to cycle number.

from SEM images. These provide easy paths for Li^+ ions during redox reactions, thereby increasing the charge storage ability of an electrode [16].

3.3. CV studies

The highly porous α-Sm_2S_3 thin film was used as a working electrode in three electrode electrochemical cell containing platinum as a counter and saturated calomel electrode (SCE) as a reference electrode. Its supercapacitive performance was tested in $LiClO_4$–PC electrolyte in a potential window of 0 to −1.2 V SCE^{-1}.

3.3.1. Effect of scan rate

Fig. 2(a) depicts cyclic voltammograms of α-Sm_2S_3 thin film electrode at different scan rates. The current under curve is increased as the scan rate increased from 5 mV s^{-1} to 100 mV s^{-1}, which show electrode behaviour identical to ideal capacitor [17]. The following relations are used [18] to obtain different capacitive values for α-Sm_2S_3 electrode,

$$C = \frac{I}{dV/dt},\ C_s = \frac{C}{W} \text{ and } C_i = \frac{C}{A} \tag{2}$$

where C, C_s, C_i stand for average, specific and interfacial capacitances, respectively and dV/dt is the scan rate, W is the weight of deposited material and A is the area of electrode dipped in an electrolyte. The variation of C_s and C_i with scan rate is shown in Fig. 2(b). The value of C_s equals to 294 F g^{-1} at a scan rate of 5 mV s^{-1}. With further increase in scan rate upto 100 mV s^{-1}, C_s is decreased to 147 F g^{-1}. This may be due to inability of inner active sites at an electrode surface to carry on redox transitions with increase in scan rate [19]. Hence, C_s obtained at lowest scan rate can be considered to be complete utilization of electrode [20].

An electrode reaction of α-Sm_2S_3 in $LiClO_4$–PC solution can be considered to be as reversible intercalation/deintercalation of Li^+ ion [21]. It can be represented as follows,

$$Sm_2S_3 + xLi^+ + xe^- \Leftrightarrow Li_xSm_2S_3 \tag{3}$$

As the Li^+ ion has lower diffusion rate in solid; the current due to electric double layer charging is dominant over faradic current peaks for Li^+ insertion/extraction and thereby no redox peaks have been appeared in cyclic voltammograms [22].

3.3.2. Effect of sulphur

To verify the contribution of sulphur to C_s, the chemically deposited pure sulphur thin film is studied for supercapacitive behaviour. Fig. 2(c) indicates cyclic voltammogram of sulphur at the scan rate of 5 mV s^{-1}. The specific capacitance of 7 F g^{-1} observed is not significant. Hence, its contribution to C_s is neglected when present as an impurity in α-Sm_2S_3 thin film.

3.3.3. Stability study

The usable limit of supercapacitive device depends upon its percentage of cycling stability. Therefore, α-Sm_2S_3 electrode was exposed to stability performance. The cyclic voltammograms of α-Sm_2S_3 electrode after 1st, 500th and 1000th cycles are indicated in Fig. 3(a). Fig. 3(b) reflects the variation of C_s as a function of cycle number. It indicates that the value of C_s is decreased from 163 to 147 F g^{-1} at the scan rate of 100 mV s^{-1} after 500 cycles. With further increase in cycling for next 500 cycles at the same scan rate, it found to be 144 F g^{-1}. Thus, supercapacitive electrode retained

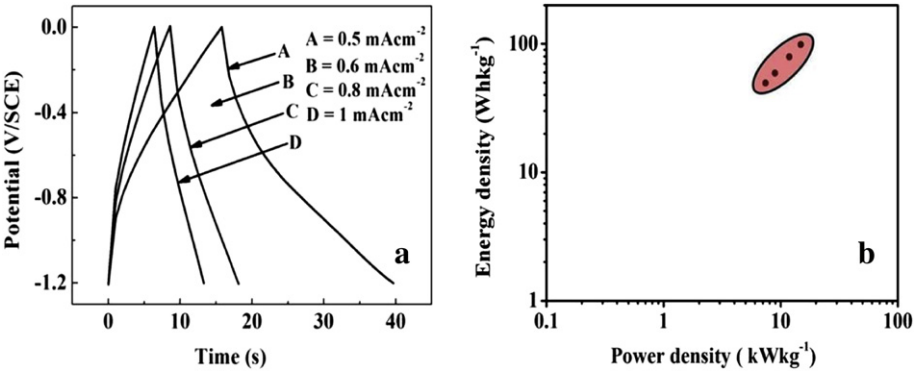

Fig. 4. (a) Galvanostatic charge–discharge curve recorded at different current densities for the α-Sm_2S_3 thin film electrode and (b) Ragone plot of α-Sm_2S_3 thin film electrode.

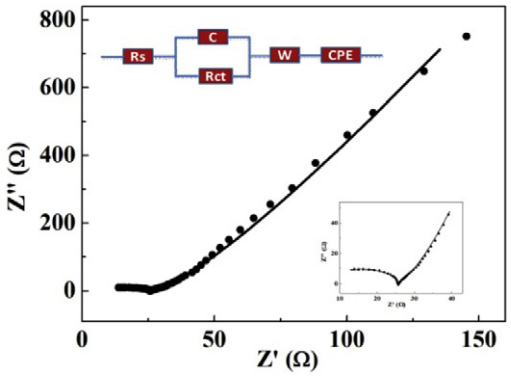

Fig. 5. The Nyquist impedance plot for α-Sm_2S_3 thin electrode. An inset at top shows an equivalent circuit diagram and that at bottom show higher frequency region of plot.

a stability of 89% after 1000 cycles. An observed decay of 11% in the C_s may be attributed to the loss of electroactive material during cycling [23].

3.4. Galvanostatic charge–discharge studies

The galvanostatic charge–discharge behaviour of α-Sm_2S_3 thin film electrode is evaluated in 1 M $LiClO_4$–PC electrolyte using three electrode system. The charging and discharging curves of α-Sm_2S_3 thin film electrode from 0 to −1.2 V SCE^{-1} at different current densities of 0.5, 0.6, 0.8, 1.0 and 2.0 mA cm^{-2} are represented in Fig. 4(a). At lowest current density of 0.5 mA cm^{-2}, the charging region is asymmetric corresponding to the discharge counterpart in the entire potential region with varying slope. Similar, behaviour was observed in case of sodium-type layered manganese oxide (Na–MnO_2) [24]. As the current density increases towards higher values, the charge and the corresponding discharge counterparts are similar, showing ideal supercapacitive behaviour [25]. The discharge curve contains the two parts, a linear one due to voltage drop across equivalent series resistance (ESR) and a nonlinear as a result of faradic reactions at an electrode surface, thereby contributing to charge storage. The variation of power density against energy density called as Ragone plot is shown in Fig. 4(b). The higher values of power and energy densities are the consequence of Li^+ ion and electron pathways on capacitive behaviour and wide potential window of 1.2 V [26].

3.5. EIS study

It is one of the fundamental tools to understand various electrochemical parameters of a supercapacitor. The same is used to obtain these parameters for α-Sm_2S_3 thin film electrode using three electrode system. The Nyquist plot for α-Sm_2S_3 thin film electrode in 1 M $LiClO_4$–PC electrolyte in the frequency range of 1 Hz–1 MHz at a polarization potential of 0.262 V with ac amplitude of 5 mV is shown in Fig. 5. The high frequency part of the plot shown at the bottom inset of Fig. 5 is indicative of equivalent series resistance (ESR) of 6.1 Ω. This arises as a result of combination of ionic resistance of electrolyte, intrinsic resistance of electrode and contact resistance between electrode and current collector [27]. The distorted semicircle involves the parallel combination charge transfer resistance (R_{ct}) and pseudocapacitance (C) due to redox reactions, whereas a line at 45° in the mid frequency range corresponds to the diffusion of Li^+ ions in the electrode represented by Warburg element (W) [28]. The constant phase element (CPE) is the consequence of non-uniform distribution of pores due to inhomogeneous charge accumulation at electrode surface. This is because, for the same frequency the penetration of ac signal is different [16]. An equivalent circuit diagram is shown at the top inset of Fig. 5. Table 1 shows fitted parameters for an assumed equivalent circuit.

Table 1
Electrochemical impedance parameters of α-Sm_2S_3 thin electrode.

Parameter	Value of parameter
C1	1.38×10^{-8}
R1	6.16
R2	19.11
Aw1	138.62
P1	2.21×10^{-4}
n1	0.94

4. Conclusions

For the first time, supercapacitive properties of α-Sm_2S_3 thin film are reported. The nanoporous morphology provided high surface area, which is useful for higher charge storage. Subsequently, high value of specific capacitance of 294 F g^{-1} is obtained. The galvanostatic charge–discharge studies show ideal capacitive behaviour of an electrode. This has been supported by EIS study. The observed high value of specific capacitance shows that α-Sm_2S_3 is a good candidate for supercapacitor application.

Acknowledgement

Authors are grateful to the Council of Scientific and Industrial Research (CSIR), New Delhi through the scheme no. 03(1165)10/EMR-II, University Grant Commission (UGC), New Delhi (India) through DSA–I program and Department of Science and Technology through DST–PURSE and FIST program for financial support.

References

[1] B.E. Conway, Electrochemical Supercapacitors, Scientific Fundamentals and Technological Applications, Kluwer Academic/Plenum Press, New York, 1999.
[2] M. Jung, K.Y. Eun, J.K. Lee, Y.J. Baik, K.R. Lee, J.W. Park, Diamond Relat. Mater. 10 (2001) 1235.
[3] J. Li, X. Wang, Q. Huang, S. Gamboa, P.J. Sebastian, J. Power Sources 158 (2006) 784.
[4] S.G. Kandalkar, J.L. Gunjakar, C.D. Lokhande, Appl. Surf. Sci. 254 (2008) 5540.
[5] S.D. Perera, B. Patel, J. Bonso, M. Grunewald, J.P. Ferraris, K.J. Balkus, ACS Appl. Mater. Interfaces 3 (2011) 4512.
[6] B.G. Choi, M. Yang, W.H. Hong, J.W. Choi, Y.S. Huh, ACS Nano 5 (2012) 4020.
[7] C.D. Lokhande, S.H. Pawar, Sol. Energy Mater. Sol. Cells 7 (1982) 313.
[8] V.V. Kaminskii, V.A. Didik, M.M. Kazanin, M.V. Romanova, S.M. Solov'ev, Tech. Phys. Lett. 35 (2009) 981.
[9] T. Zhu, Z. Wang, S. Ding, J.S. Chen, X.W. Lou, RSC Adv. 1 (2011) 397.
[10] F. Tao, Y.Q. Zhao, G.Q. Zhang, H.L. Li, Electrochem. Commun. 9 (2007) 1282.
[11] A. Jayaraman, V. Narayanamurti, E. Bucher, R.G. Maines, Phys. Rev. Lett. 25 (1970) 1430.
[12] R.C. Vickery, H.M. Muir, Energy Convers. Manage. 1 (1969) 179.
[13] S.B. Jundale, C.D. Lokhande, Sol. Energy Mater. Sol. Cells 28 (1992) 151.
[14] R. Suryanarayanan, G. Brun, Thin Solid Films 35 (1976) 263.
[15] U.M. Patil, R.R. Salunkhe, K.V. Gurav, C.D. Lokhande, Appl. Surf. Sci. 255 (2008) 2603.
[16] D. Hulicova, M. Kodama, H. Hatori, Chem. Mater. 18 (2006) 2318.
[17] C.C. Hu, T.W. Tsou, Electrochem. Commun. 4 (2002) 105.
[18] B.E. Convey, W.G. Pell, in: Proceedings of the Eighth International Seminar on Double Layer Capacitors and Similar Energy Storage Devices, Deerfiled Beach, FL (December 1998).
[19] V.S. Kumbhar, A.D. Jagadale, N.M. Shinde, C.D. Lokhande, Appl. Surf. Sci. 259 (2012) 39.
[20] T.P. Gujar, W. Kim, I. Puspitasari, K.D. Jung, O.S. Joo, Int. J. Electrochem. Sci. 22 (2007) 666.
[21] M. Manickam, P. Singh, T.B. Issa, S. Thurgate, R.D. Marco, J. Power Sources 130 (2004) 254.
[22] A. Yuan, Q. Zhang, Electrochem. Commun. 8 (2006) 1173.
[23] W.C. Chen, C.C. Hu, C.C. Wang, C.K. Min, J. Power Sources 82 (2004) 292.
[24] X. Yang, G. Wang, R. Wang, X. Li, Electrochim. Acta 55 (2010) 5414.
[25] S. Chen, J. Zhu, Q. Han, Z. Zheng, Y. Yang, X. Wang, Cryst. Growth Des. 9 (2009) 4356.
[26] B.G. Choi, M.H. Yang, W.H. Hong, J.W. Choi, Y.S. Huh, ACS Nano 6 (2012) 4020.
[27] A. Bruke, J. Power Sources 91 (2000) 37.
[28] Z. Lei, F. Shi, Li. Lu, ACS Appl. Mater. Interfaces 4 (2012) 1058.